Robotica (2000) volume 18, pp. 429–441. Printed in the United Kingdom © 2000 Cambridge University Press

A fast procedure for computing incremental growth distances

Sun-Mog Hong*, Joon-Hyuek Yeo** and Hae-Wook Park†

(Received in Final Form: July 9, 1999)

SUMMARY

A fast numerical procedure is presented for computing growth distances between a pair of polytopes in three dimensional space that move incrementally along specified smooth paths. The procedure carrys out the growth distance evaluations efficiently by predicting and verifying contact configurations between a pair of grown polytopes. In the prediction and verification the procedure uses vertex and facial characterizations of polytopes and exploits their geometric adjacency information. The computation time, in average, is very small and does not depend significantly on the geometric complexity of two polytopes. A numerical example is presented to demonstrate the applicability of the procedure to interference detection in robotic simulations.

KEYWORDS: Growth distance; Incremental distance; Interference detection; Robotic simulations

1. INTRODUCTION

Recently, new quantitative measures of object separation and penetration, called growth distances, have been introduced by Gilbert and Ong.[1,2] The growth distances are defined for a pair of convex objects. They are a measure of how much each of the objects must be grown, outward from fixed seed points in their interiors, so that they just touch. One important aspect of the growth distances is in that, when a pair of object models intersect each other, they can quantify depth of the intersection and provide information on changes in objects position which can reduce or eliminate the intersection. Besides many desirable properties, their principal advantage is from computational simplicity and speed. For a pair of polytopal objects in three dimensional space, the growth distance is computed by solving a simple linear programming problem. In particular, the speed advantage is significant for penetration distance, compared to translational penetration measures (see Ref. 2 for a review of translational penetration measures and their references). Consequently, their advantages are significant in a variety of applications:[2–5] robot path-finding in the presence of obstacles; and interference detection in computer-aided design and computer graphics.

In these applications, it is often necessary to compute the growth distances between a pair of objects as they move incrementally along a specified geometric path. Specifically, it is necessary to carry out the growth distance calculations on a closely spaced grid of points along the path. Since number of grid points along the path may be large, it is important to minimize the overall computational time. It has been noted[1,2] that the closeness of the grid points can be exploited to reduce the overall computational time. The incremental scheme in Ref. 2 uses good initializations based on the growth distance computation before the motion increment. It gives faster computations without using structural information about the objects, but the time still increases linearly with object complexity. Near-constant time results can be obtained by utilizing structural information on the adjacency of faces and/or vertices. Ong and Huang[6] achieved this improvement in speed by using only facial and their adjacency information. The advantage of adjacency structures was first introduced by Lin and Canny[7] in computations of incremental Euclidean distances. Lin and Canny[7] used full structural information consisting of vertex, edge and facial as well as their adjacency information. See also references 8–10.

In this paper we present an efficient procedure for computing the growth distances on a closely spaced grid of points along a specified smooth path. This procedure carrys out the growth distance evaluations efficiently by predicting and verifying contact configurations between a pair of grown polytopal objects. In the prediction and verification the procedure uses vertex and facial characterizations of polytopes and exploits their geometric adjacency information. Preprocessing of the data structure is required for the procedure. For small incremental motions between grid points, the prediction is almost always correct and the total computational time for the entire sequence of points is significantly reduced. The total computational time does not depend significantly on the geometric complexity of two polytopes. For an asymptotic case where motion increments are sufficiently small, the procedue requires approximately 20% less arithematic operations than Ong and Huang's[6] version.

The organization of this paper is as follows; Section 2 reviews the definition of growth distance and some related issues. Our algorithmic procedure, including the subprocedues for the prediction and verification, and its computational complexity are discussed in Section 3. In Section 4, results of extensive numerical experiments on our procedure are presented to show its computational advantage in speed and to demonstrate its applicability to robotic simulations.

The following is a summary of basic notations and definitions. They and the notations in subsequent sections

* School of Electronic and Electrical Eng., Kyungpook National University, Taegu 702-701 (Korea).
E-mail: smhong@ee.kyungpool.ac.kr
** Hyundai Heavy Industries Co. Ltd., San 1-8, Mabook-ri, Yongin-shi, Kyunggi-do 449-716 (Korea).
E-mail: riverman@hhi.co.kr
† Brain Co. Ltd., 1-3-11 Omika-cho, Hitachi-shi, Ibaraki-ken 319-1221 (Japan). E-mail: phw0119@hotmail.com

https://doi.org/10.1017/S0263574799001939 Published online by Cambridge University Press

agree with those given in reference 2. The empty set is ϕ; the non-negative real numbers are R^+; $x, y \in R^n$ are column vectors with real components; vector and matrix transposes are indicated by a superscript T. The interior and relative interior[11] of a set $A \subset R^n$ are, respectively, *int A* and *ri A*. The Minkowski sum or difference of $A, B \subset R^n$ is $A \pm B = \{a \pm b : a \in A, b \in B\}$. The multiplication of A by a scaler $\sigma \in R$ is $\sigma A = \{\sigma a : a \in A\}$. $SO(n)$ is the special orthogonal group of real $n \times n$ orthogonal matrices with determinant one, *i.e.*, $T \in SO(n)$ is a rotation matrix. The hyperplane in R^n passing through p with normal $\eta \neq 0$ is $P(p, \eta) = \{x : \eta^T(x-p) = 0\}$; the half space bounded by $P(p, \eta)$ with outward normal η is $H(p, \eta) = \{x : \eta^T(x-p) \leqslant 0\}$. A and B are said to be *separated* if there exists a separating hyperplane $P(p, \eta)$ such that $A \subset H(p, \eta)$ and $B \subset H(p, -\eta)$; A and B are said to be *regularly* separated if $A \cap B$ is a singleton and the hyperplane which seperates A and B is unique. The cardinality of the index set I is $|I|$.

The class of sets in R^n that are compact, convex and have a non-empty interior is denoted by O. O is the natural class of sets for modeling convex objects. In the representation of objects $n = 3$. If the object $A \in O$ undergoes a rotation $T \in SO(3)$ followed by a translation $s \in R$, it is represented by $TA + \{s\}$.

2. PRELIMINARIES

In this section, we review briefly the definition of growth distance and some related issues. (See reference 2 for details). The growth distance between a pair of objects, $A, B \in O$, is a measure of how much each of the objects must be grown outward, from fixed seed points in their interiors, so that they just touch. The fractional growth required for touching is called the growth function. When it is scaled appropriately it generates both the separation and penetration growth distances.

The growth models for the objects $A \in O$ and $B \in O$ are given by $A(\sigma) = \{p_A\} + \sigma\bar{A}$ and $B(\sigma) = \{p_B\} + \sigma\bar{B}$, where $\bar{A} = A - \{p_A\}$, $\bar{B} = B - \{p_B\}$, and p_A and p_B satisfy the conditions $p_A \in int\, A$, $p_B \in int\, B$. For $\sigma = 1$, the original objects are obtained, *i.e.*, $A(1) = A$ and $B(1) = B$; for $\sigma < 1$, the objects contract about their respective seed points; for $\sigma > 1$, the objects expand about their respective seed points. The growth function for the object pair is defined by

$$g(A, B) = \sigma^* = min\{\sigma \in R^+ : A(\sigma) \cap B(\sigma) \neq \phi\} \qquad (1)$$

Geometrically, the growth funtion is the value of σ such that $A(\sigma)$ and $B(\sigma)$ just touch. If $g(A, B) < 1$, objects A and B must be contracted so that they just touch. In fact, $g(A, B) < 1$ if and only if $int\, A \cap int\, B \neq \phi$. Similarly, $g(A, B) > 1$ means that A and B are strictly separated. Obviously, $g(A, B) - 1$ is a numerical measure of separation and penetration whose sign distinguishes separation and penetration. A penetration distance is obtained by scaling $1 - g(A, B)$ according to the size of A and B. For example, the scaling factor was chosen in reference 2 by $R_A + R_B$, where R_A and R_B are radii of circumscribing spheres for the sets $\bar{A}$ and $\bar{B}$, respectively.

Figure 1 shows a geometric configuration of $A(\sigma)$ and $B(\sigma)$ at σ^*. As indicated in the figure, $A(\sigma^*)$ and $B(\sigma^*)$ are separated by a hyperplane $P(x^*, \eta^*)$ passing through the corresponding point of contact $x^* \in A(\sigma^*) \cap B(\sigma^*)$. The *optimal* configuration of the two grown objects at σ^* corresponds to the existence of a seperating hyperplane between $A(\sigma^*)$ and $B(\sigma^*)$ and that of the optimal point x^*.[1,2]

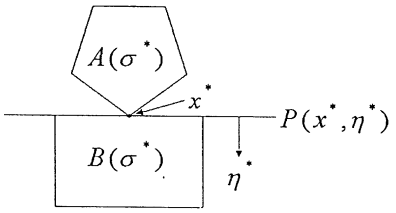

Fig. 1. Geometric configuration of $A(\sigma^*)$ and $B(\sigma^*)$.

When A and B are convex polytopes the computation of $g(A, B)$ is simple. In this situation $\bar{A}$ and $\bar{B}$ are polytopes which can be characterized respectively by

$$\bar{A} = \{x : \gamma_i^T x \leqslant 1, i \in \mathcal{F}_A\} \text{ and } \bar{B} = \{x : \gamma_i^T x \leqslant 1, i \in \mathcal{F}_B\} \qquad (2)$$

Here $\mathcal{F}_A$ and $\mathcal{F}_B$ are the index sets which designate each face of $\bar{A}$ and $\bar{B}$, respectively. $|\mathcal{F}_A|$ and $|\mathcal{F}_B|$ are respectively the number of "faces" of $\bar{A}$ and $\bar{B}$. It then follows that $A(\sigma) = \{x : \gamma_i^T x - \sigma \leqslant \delta_i, i \in \mathcal{F}_A\}$, where $\delta_i = \gamma_i^T p_A$, and $B(\sigma) = \{x : \gamma_i^T x - \sigma \leqslant \delta_i, i \in \mathcal{F}_B\}$, where $\delta_i = \gamma_i^T p_B$. Using this characterization of $A(\sigma)$ and $B(\sigma)$, $\sigma^* = g(A, B)$ and $x^* \in A(\sigma^*) \cap B(\sigma^*)$ can be found by solving the linear programming problem:

$$min\ \sigma,\ (x, \sigma) \in R^{n+1} \qquad (3)$$

subject to $\gamma_i^T x - \sigma \leq \delta_i$, $i \in \mathcal{F} = \mathcal{F}_A \cup \mathcal{F}_B$, where $\delta_i = \gamma_i^T p_A$, $i \in \mathcal{F}_A$, and $\delta_i = \gamma_i^T p_B$, $i \in \mathcal{F}_B$. It is well known that such a linear programming problem can be solved in $O(|\mathcal{F}|)$ time.[13]

Suppose that the objects A and B undergo rigid-body motions along paths specified by $t \in R$. The rigid-body motions of the objects can be described in general by a quadruple $(T_A(t), s_A(t), T_B(t), s_B(t))$. More specifically, let $\bar{A}$ and $\bar{B}$ be the objects in their base positions with the origin being their seed points, *i.e.*, $p_A = 0$ and $p_B = 0$. Correspondingly, we can represent the objects moved along the paths and grown by σ as:

$$A(\sigma, t) = \sigma T_A(t)\bar{A} + \{s_A(t)\} \text{ and } B(\sigma, t) = \sigma T_B(t)\bar{B} + \{s_B(t)\}. \qquad (4)$$

When they are grown until they just touch, they determine $\sigma^*(t)$ and $x^*(t)$, the growth required for touching and a corresponding point of contact. Obviously, $A(\sigma^*(t), t)$ and $B(\sigma^*(t), t)$ represent respectively the grown objects, and $int\, A(\sigma^*(t), t) \cap int\, B(\sigma^*(t), t) = \phi$, $x^*(t) \in A(\sigma^*(t), t) \cap B(\sigma^*(t), t)$.

In the sequel, we assume that $\bar{A}$ and $\bar{B}$ are polytopes with $p_A = 0$ and $p_B = 0$, respectively.

3. COMPUTATIONAL PROCEDURES FOR INCREMENTAL GROWTH DISTANCES

We are interested in how $\sigma^*(t)$ and $x^*(t)$ behave as $t = t_k, t_{k+1}, \ldots$, etc. Specifically, we wish to determine C, the configuration of the contact. The configuration defines the geometric nature of the contact between $A(\sigma^*(t), t)$ and $B(\sigma^*(t), t)$ in R^3. If the contact configuration has been

https://doi.org/10.1017/S0263574799001939 Published online by Cambridge University Press

determined, the computations of $\sigma^*(t)$ and $x^*(t)$ are straightforward.

Geometrically, the contact features in each grown polytopal object can be vertex (V), edge (E) or face (F). The geometric *configuration* is the specific feature pair at contact. The generic contact pairs are *VF* and (non-collinear) *EE*. The nongeneric pairs *VE* and *EF* are much more likely to occur than the remaining nongeneric pairs *VV*, *FF* and (collinear) *EE*. In fact, *VE* and *EF* represent the *generic transitions* between one generic configuration and the next generic configuration; *i.e.*, if $\bar{t}$ is a transition time, where the configurations at $\bar{t}-\varepsilon$ and $\bar{t}+\varepsilon(\varepsilon>0$ and sufficiently small) are different, then the generic transition at $\bar{t}$ is either *VE* or *EF*. Suppose, for example, that the configuration *VF* undergoes a transition. The *EF* transition takes place when an edge of $A(\sigma^*(t), t)$, adjacent to the vertex V_i moves into a face of $B(\sigma^*(t), t)$ while V_i remains in the interior of the face; see Figure 2. There are two ways in which these *EF* trasitions can happen; see Figure 3. The *VE* transition takes place when V_i moves to an edge of the face F_j while $A(\sigma^*(t), t)$ and $B(\sigma^*(t), t)$ remain strictly separated; see Figure 4. A similar discussion can be given for the transition from (non-collinear) *EE*.

Now suppose we know C^-, the contact configuration at $\bar{t}-\varepsilon$. Given the configuration C^-, what is C^+, the configuration at $\bar{t}+\varepsilon$? This is the *prediction* problem. If the object motions are continuous and $t=t_k$, t_{k+1} represent grid points along the motion, the validity of prediction from t_k to t_{k+1} depends on $\Delta t=t_{k+1}-t_k$. If Δ_t is sufficiently small and C^- and C^+ are generic, prediction of C^+ from C^- is possible.

Often there is no transition between C^- and C^+: for Δt small it is usually true that $C^-=C^+$. Computational procedures are required to verify the hypothesis that $C^-=C^+$: given the pair $(\sigma^*(t_k), x^*(t_k))=(\sigma_k^*, x_k^*)$ which is *feasible* ($x_k^*\in A(\sigma_k^*, t_k)\cap B(\sigma_k^*, t_k)$) and *optimal* (there is a separating plane between $A(\sigma_k^*, t_k)$ and $B(\sigma_k^*, t_k)$ passing through x_k^*), it is required to test whether or not the

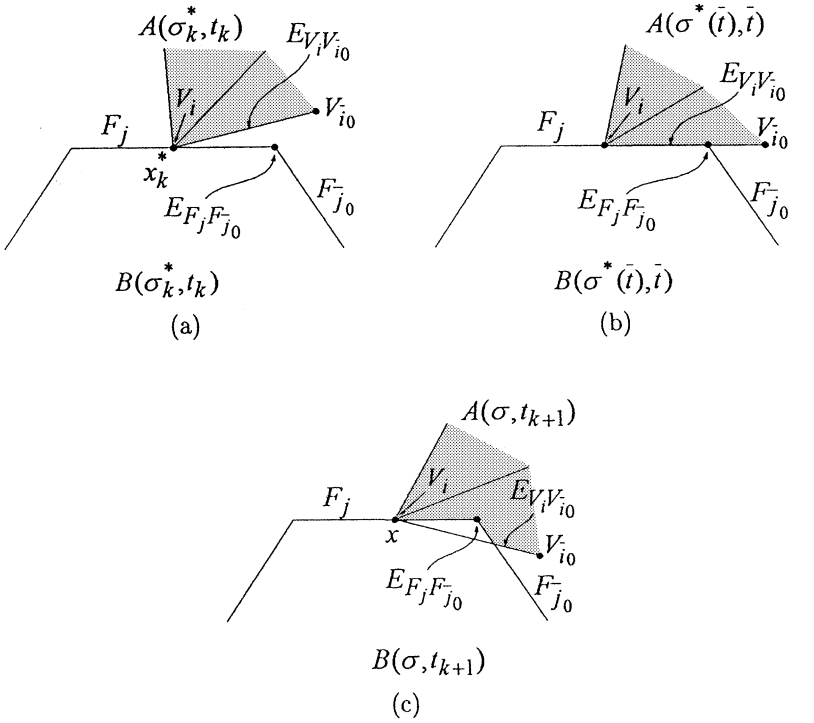

Fig. 2. View along $E_{F_jF_{j0}}$ for *VF* loss of optimality. (a) $t=t_k$. (b) $t=\bar{t}$. (*c*) $t=t_{k+1}$.

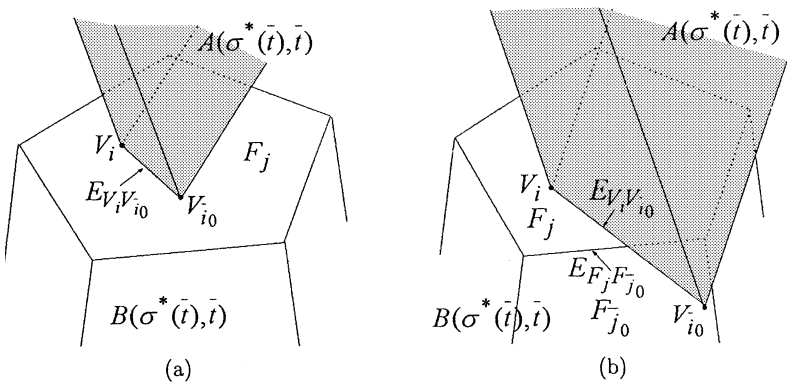

Fig. 3. *EF*-type transition contacts at $t=\bar{t}$.

https://doi.org/10.1017/S0263574799001939 Published online by Cambridge University Press

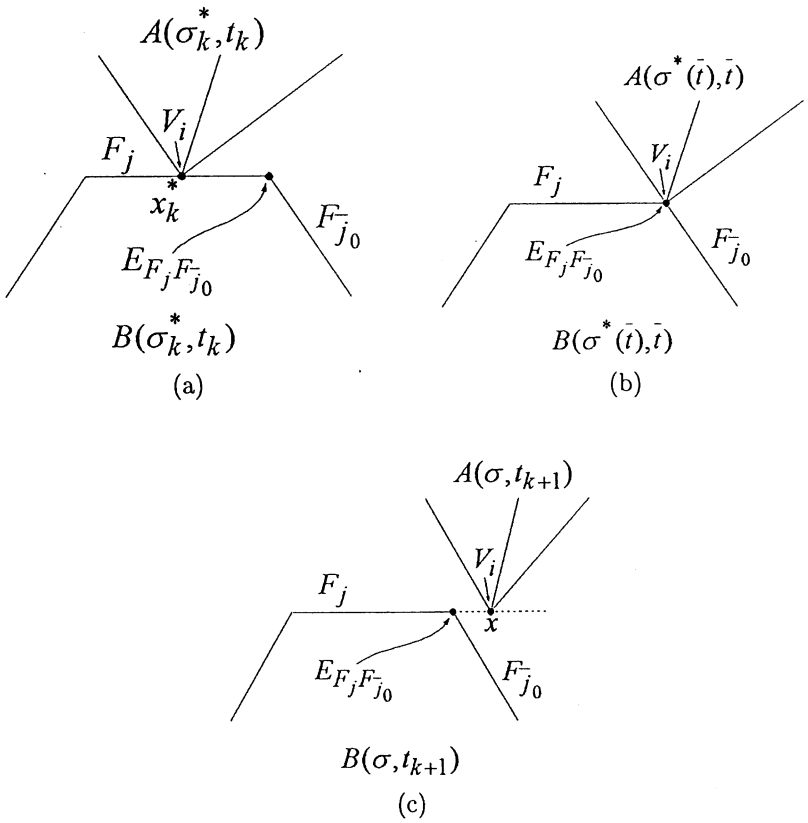

Fig. 4. View along $E_{F_j F_{\bar{j}_0}}$ for *VF* loss of feasibility. (a) $t = t_k$. (b) $t = \bar{t}$. (*c*) $t = t_{k+1}$.

configuration C^- determines a feasible and optimal pair at t_{k+1}. In particular, does there exist (σ, x) such that $x \in A(\sigma, t_{k+1}) \cap B(\sigma, t_{k+1})$ and there is a separating plane between $A(\sigma, t_{k+1})$ and $B(\sigma, t_{k+1})$ passing through x? These tests procedures, which are simple and computationally inexpensive, are described in Section 3.1.

Even if the test procedures indicate $C^- \neq C^+$, we can predict a "likely" C^+ using the data available from C^- and the test procedures. It is based on the assumption that Δt is small and that there is *only* one transition time $\bar{t}$, $t_k < \bar{t} < t_{k+1}$. In practice, there is no easy way to determine if Δt is sufficiently small, so the prediction is C^+: the prediction C may not equal C^+. We hope in most cases that C is not indeed C^+. Then, restart steps (steps of the active set approach[13] for solving the full linear programming problem (3)), which are computationally expensive, will only be needed occasionally. The prediction procedures are discussed in Sections 3.2 and 3.3. In Sections 3.1–3.3, we assume that contact configurations C^- and C^+ are generic. We can relax this assumption, but from a practical point of view it seems not worth the added algorithmic complexity that relaxing the assumption requires. Section 3.4 describes our algorithmic steps for computing incremental growth distances which use the test and prediction procedures as substeps.

To proceed to further discussion, we need some additional notations to represent input data for polytopal objects. The input data required for our procedures include the facial and vertex information and their geometric adjacency information. Thus, in addition to the facial characterization of (2) we need a vertex characterization. Specifically, a polytope $\bar{A}$ can be characterized by the convex hull of its vertices:

$$\bar{A} = co\{v_i : i \in \mathcal{V}_A\}. \tag{5}$$

Here, v_i denotes the coodinates of a vertex V_i and $\mathcal{V}_A$ is the index set which designates each vertex of $\bar{A}$. The characterizations of the polytopes by (2) and (5) are minimal in the sense that removal of any inequality or vertex forces a change in $\bar{A}$ and $\bar{B}$. We will represent the information of the face adjacency by the following index to index set maps: for $i \in \mathcal{V}_A$, $\mathcal{V}_A^i = \{\bar{i} : \bar{i}$ is the index adjacent to the vertex $V_i\}$; for $j \in \mathcal{F}_A$, $\mathcal{F}_A^j = \{\bar{j} : \bar{j}$ is the index of face adjacent to the face $F_j\}$ where F_j denotes a face of $\bar{A}$ designated by the index j. Clearly, $\mathcal{V}_A^i \subset \mathcal{V}_A$ and $\mathcal{F}_A^j \subset \mathcal{F}_A$. Tables of indices can be implemented for the index to index set map. An edge of $\bar{A}$ can be described either in terms of a corresponding face pair or a corresponding vertex pair interchangeably. Because edges are uniquely defined, there is a one-to-one correspondence between their face pairs and vertex pairs. We also need tables of indices for these functions.

The *VF* configuration between V_i, $i \in \mathcal{V}_A$ and F_j, $j \in \mathcal{F}_B$ will be represented by $C = V_i F_j$. Similarly, $C = F_i V_j$ represents the *FV* configuration between F_i, $i \in \mathcal{F}_A$ and V_j, $j \in \mathcal{V}_B$. $C = E_{V_{i_1} V_{i_2}} E_{F_{j_1} F_{j_2}}$ represents the *EE* configuration between the edge defined by a pair of adjoining vertices V_{i_1}, $i_1 \in \mathcal{V}_A$, and V_{i_2}, $i_2 \in \mathcal{V}_A^{i_1}$, and the edge defined by a pair of adjoining faces F_{j_1}, $j_1 \in \mathcal{F}_B$, and F_{j_2}, $j_2 \in \mathcal{F}_B^{j_1}$.

3.1. Tests of contact configurations

Consider the test procedure for the generic configuration $C = V_i F_j$ at t_{k+1}. The pair (σ, x) is determined from the

https://doi.org/10.1017/S0263574799001939 Published online by Cambridge University Press

condition that the vertex V_i of $A(\sigma, t_{k+1})$ belongs to the facial plane containing the face F_j of $B(\sigma, t_{k+1})$, *i.e.*,

$$(\sigma T_A^+ v_i + s_A^+) \in \{ y : T_B^+ \gamma_j)^T (y - s_B^+) = \sigma \}. \quad (6)$$

The condition gives

$$\sigma = \frac{(T_B^+ \gamma_j)^T (s_A^+ - s_B^+)}{1 - (T_B^+ \gamma_j)^T (T_A^+ v_i)} \text{ and } x = \sigma T_A^+ v_i + s_A^+. \quad (7)$$

Here, T and s with the subscript $+(-)$ denote the corresponding quantities computed for $t_{k+1}(t_k)$. Then *feasibility* is determined by confirming that x belongs to the relative interior of the face F_j of $B(\sigma, t_{k+1})$, *i.e.*,

$$(T_B^+ \gamma_j)^T (x - s_B^+) < \sigma, \bar{j} \in \mathcal{F}_B^j. \quad (8)$$

The regular separation (of the grown sets) of the generic configuration at t_{k+1} can be described in terms of the tangent cones of the objects defined by C and their corresponding normal cones[11]. For $C = V_i F_j$, the tangent cone of $A(\sigma, t_{k+1})$ at x is $TC_A^+(V_i) = \{\Delta x = T_A^+ (\Sigma_{\bar{i} \in V_A^i} \lambda_{\bar{i}} (v_{\bar{i}} - v_i)) : \lambda_{\bar{i}} \geqslant 0, \bar{\imath} \in v_A^i\}$, and the tangent cone of $B(\sigma, t_{k+1})$ at x is $TC_B^+(F_j) = \{\Delta x : (T_B^+ \gamma_j)^T \Delta x \leqslant 0\}$, a half space. At t_{k+1} these tangents cones, which are local description of $A(\sigma, t_{k+1})$ and $B(\sigma, t_{k+1})$ at x, are separated if there exists $\eta \neq 0$ such that $\eta^T \Delta x \geq 0$ for all $\Delta x \in TC_A^+(V_i)$ and $\eta^T \Delta x \leq 0$ for all $\Delta x \in TC_B^+(F_j)$. Note that η is a normal to a seperating plane. The regular seperation is expressed more directly in terms of the relative interiors of the normal cones: $riNC_A^+(V_i) = \{ y : y^T \Delta x < 0$ for all $\Delta x \in TC_A^+(V_i)\} = \{ y : y^T T_A^+ (v_{\bar{\imath}} - v_i) < 0$ for all $\bar{i} \in \mathcal{V}_A^i\}$ and $riNC_B^+(F_j) = \{ y : y^T \Delta x < 0$ for all $\Delta x \in TC_B^+(F_j)\} = \{y : y = \lambda T_B^+ \gamma_j, \lambda > 0\}$. Specifically, $TC_A^+(V_i)$ and $T_B^+(F_j)$ are separated regularly if $riNC_A^+(V_i) \cap -riNC_B^+(F_j) \neq \phi$; $-T_B^+ \gamma_j \in riNC_A^+(V_i)$ is the requirement for regular seperation of $TC_A^+(V_i)$ and $TC_B^+(F_j)$. Thus, it is clear that the regular seperation is checked by showing that

$$(-T_B^+ \gamma_j)^T T_A^+ (v_{\bar{i}} - v_i) < 0, \bar{\imath} \in \mathcal{V}_A^i. \quad (9)$$

The pair (σ, x) for $V_i F_j$ configuration is *optimal* if both feasibility and regular separation conditions are satisfied. Specifically: if the conditions (8), (9) are satisfied, then it is verified that $C = C^+$, and the pair (σ, x) of (7) is feasible and optimal; otherwise, it turns out that $C \neq C^+$. If $C = C^-$ and it turns out $C \neq C^+$, there must be a transition between t_k and t_{k+1}, almost certainly of the *EF* or *VE* type.

The test procedure for a generic *EE* configuration is also simple. Let v_{A_1}, v_{A_2} and γ_{A_1}, γ_{A_2} denote a pair of vertex coordinates and a pair of face normals, respectively, defining the contact edge of $\bar{A}$. Similarly, let v_{B_1}, v_{B_2} and γ_{B_1}, γ_{B_2} represent the corresponding data for $\bar{B}$. Also, let e_A and e_B denote the edge vectors $v_{A_2} - v_{A_1}$ and $v_{B_2} - v_{B_1}$, respectively. The line extending from the edge of $A(\sigma, t_{k+1})$ is given by

$$\{ y : y = \sigma T_A^+ ((1 - \lambda_A)\, v_{A_1} + \lambda_A\, v_{A_2}) + s_A^+, \lambda_A \in R\}, \quad (10)$$

or, it can be given in term of the intersection of a pair of corresponding facial planes by

$$\{ y : (T_A^+ \gamma_{A_i})^T (y - s_A^+) = \sigma, i = 1, 2\}. \quad (11)$$

Similarly, the line extending form the edge of $B(\sigma, t_{k+1})$ is given by

$$\{ y : y = \sigma T_B^+ ((1 - \lambda_B)\, v_{B_1} + \lambda_B v_{B_2}) + s_B^+, \lambda_B \in R\}, \quad (12)$$

or,

$$\{ y : (T_B^+ \gamma_{B_i})^T (y - s_B^+) = \sigma, i = 1, 2\}. \quad (13)$$

The pair (σ, x) and λ_A, λ_B at x are computed as the intersection of the two lines. Substituting (10) into two equations in (13), we obtain the two equations which determine σ^{-1} and λ_A:

$$q_{0_i} \frac{1}{\sigma} + q_{1_i} \lambda_A = -q_{2_i}, i = 1, 2 \quad (14)$$

where $q_{0_i} = (T_B^+ \gamma_{B_i})^T (s_A^+ - s_B^+)$, $q_{1_i} = (T_B^+ \gamma_{B_i})^T T_A^+ e_A$, $q_{2_i} = (T_B^+ \gamma_{B_i})^T T_A^+ v_{A_1} - 1$. Once σ is obtained, it is possible to obtain λ_B by solving either one of the following two equations (obtained by substituting (12) into the two equations in (11))

$$q_{3_i} \frac{1}{\sigma} + q_{4_i} \lambda_B = -q_{5_i}, i = 1, 2 \quad (15)$$

where $q_{3_i} = (T_A^+ \gamma_{A_i})^T (s_B^+ - s_A^+)$, $q_{4_i} = (T_A^+ \gamma_{A_i})^T T_B^+ e_B$, $q_{5_i} = (T_A^+ \gamma_{A_i})^T T_B^+ v_{B_1} - 1$. As a result, a set of conditions for feasibility at t_{k+1} can be stated in terms of λ_A and λ_B:

$$\lambda_A > 0, \quad (16)$$

$$\lambda_A - 1 < 0, \quad (17)$$

$$\lambda_B > 0, \quad (18)$$

$$\lambda_B - 1 < 0, \quad (19)$$

We also need to assure that the tangent cones of $A(\sigma, t_{k+1})$ and $B(\sigma, t_{k+1})$ at the point x of edge-edge contact remain regularly separated to assure that indeed the optimality of the σ determination holds. For the *EE* configuration, the relative interiors of the normal cones are $riNC_A^+(E_{F_{A_1} F_{A_2}}) = \{ y : y = T_A^+ (\alpha_1 \gamma_{A_1} + \alpha_2 \gamma_{A_2}),\ \alpha_1 > 0,\ \alpha_2 > 0\}$ and $riNC_B^+(E_{F_{B_1} F_{B_2}}) = \{ y : y = T_B^+ (\beta_1 \gamma_{B_1} + \beta_2 \gamma_{B_2}),\ \beta_1 > 0,\ \beta_2 > 0\}$. The regular separation required of the two fan-like tangent cones is equivalent to $riNC_A^+(E_{F_{A_1} F_{A_2}}) \cap -riNC_B^+(E_{F_{B_1} F_{B_2}}) \neq \phi$. Specifically, there must exist positive numbers α_1, α_2, β_1, β_2 such that

$$\mathbf{r}^+ = T_A^+ (\alpha_1 \gamma_{A_1} + \alpha_2 \gamma_{A_2}) = -T_B^+ (\beta_1 \gamma_{B_1} + \beta_2 \beta_{B_2}), \quad (20)$$

where $\mathbf{r}^+$ denotes a normal vector to the plane determined by the two edges. Since $\gamma_{B_i}^T e_B = 0$, $i = 1, 2$, it follows that

$$(\mathbf{r}^+)^T T_B^+ e_B = \alpha_1 (T_A^+ \gamma_{A_1})^T T_B^+ e_B + \alpha_2 (T_A^+ \gamma_{A_2})^T T_B^+ e_B = 0. \quad (21)$$

Thus, it must hold that

$$\frac{\alpha_2}{\alpha_1} = -\frac{(T_A^+ \gamma_{A_1})^T T_B^+ e_B}{(T_A^+ \gamma_{A_2})^T T_B^+ e_B} > 0. \quad (22)$$

Similarly, from $\gamma_{A_i}^T e_A = 0$, $i = 1, 2$, it follows that

$$(\mathbf{r}^+)^T T_A^+ e_A = \beta_1 (T_B^+ \gamma_{B_1})^T T_A^+ e_A + \beta_2 (T_B^+ \gamma_{B_2})^T T_A^+ e_A = 0, \quad (23)$$

and it must hold that

$$\frac{\beta_2}{\beta_1} = -\frac{(T_B^+ \gamma_{B_1})^T T_A^+ e_A}{(T_B^+ \gamma_{B_2})^T T_A^+ e_A} > 0. \quad (24)$$

https://doi.org/10.1017/S0263574799001939 Published online by Cambridge University Press

In addition to (22) and (24), the regular separation of the *EE* configuration requires

$$\left(T_A^+\left(\gamma_{A_1}+\frac{\alpha_2}{\alpha_1}\,\gamma_{A_2}\right)\right)^T\left(-T_B^+\left(\gamma_{B_1}+\frac{\beta_2}{\beta_1}\,\gamma_{B_2}\right)\right)>0. \quad (25)$$

If both the feasibility conditions (16)–(19) and the regular separation conditions (22), (24) and (25) are satisfied, then it is verified that $C=C^+$, and the pair (σ, x) is feasible and optimal; otherwise, it turns out that $C\neq C^+$. If $C=C^-$ and it turns out that $C\neq C^+$, there must be a transition between t_k and t_{k+1}, almost certainly of the *EF* or *VE* type.

3.2. Prediction for non-optimal configurations

Suppose that the test procedures are entered at t_{k+1} with a *VF* configuration C^-. Using C^- with the object data at t_{k+1}, compute (7) for (σ, x) and test the feasibility conditions (8) and the regular separation conditions (9). If the *VF* configuration is feasible but *not* regularly seperated (not optimal), it follows that a transition has occurred between t_k and t_{k+1}. Generically, the transition is of the *EF* type and leads to a *VF* or *EE* type configuration. A similar argumant also holds for the case that C^- is an *EE* configuration.

We will discuss the procedures for determining the prediction C for the *EF*-type transition. First, consider the geometric situation corresponding to loss of optimality of a *VF* configuration, which is shown in Figure 2. The *VF* configuration C^- applied at t_{k+1} gives (σ, x) where the vertex V_i belongs to the relative interior of the face F_j, but the edge $E_{V_iV_{i_0}}$ penetrates below the face F_j. The transition configuration at $t=\bar{t}$ is generically of the *EF* type. For $A(\sigma, t_{k+1})$ and $B(\sigma, t_{k+1})$ to touch it is clear that σ must decrease; when they do touch the likely generic configurations are $V_{\bar{i}_0}F_j$ or $E_{V_iV_{i_0}}E_{F_jF_{\bar{j}_0}}$. The configuration V_iF_j is impossible because the decrease in σ means V_i is not contained in the facial plane of F_j. Note that the vertex $V_{\bar{i}_o}$ is predicted by an inequality in (9) which is *violated* by the loss of optimality, *i.e.*, $V_{\bar{i}_0}$ is a vertex adjacent to V_i and $(-T_B^+\gamma_j)^TT_A^+(v_{\bar{i}_0}-v_i)>0$. We assume implicitly that only one of the inequalities (9) is violated, *i.e.*, $(-T_B^+\gamma_j)^T T_A^+(v_{\bar{i}}-v_i)<0$, $\bar{i}\in\mathcal{V}_A^i$, $\bar{i}\neq\bar{i}_0$. Generically, this is the situation if Δt is sufficiently small.

More specifically, consider the geometric situation at the transition time $\bar{t}$; see Figure 3. The edge $E_{V_iV_{i_0}}$ is lying on the facial plane containing the face F_j. If Δt is sufficiently small, the vertex V_i belongs to the relative interior of the face F_j. Then, generically there are two possible cases: the edge $E_{V_iV_{i_0}}$ is included in the relative interior of the face F_j (see Figure 3(a)); and the edge $E_{V_iV_{i_0}}$ crosses an edge defined by the face F_j and a face $F_{\bar{j}_0}$, $\bar{j}_0\in\mathcal{F}_B^j$ (see Figure 3(b)). The first case implies the contact between the vertex $V_{\bar{i}_0}$ and the face of F_j at $t+\varepsilon$ as a result of the *EF*–type transition; the second implies the contact between the edge $E_{V_iV_{i_0}}$ and the edge $E_{F_jF_{j_0}}$. Thus, under the assumption that Δt is sufficiently small, we assume that the first case has occurred if the edge $E_{V_iV_{i_0}}$ of $A(\sigma, t_{k+1})$ does not puncture any one of the faces $F_{\bar{j}}$, $\bar{j}\in\mathcal{F}_B^j$, of $B(\sigma, t_{k+1})$, and we predict the configuration $V_{\bar{i}_0}F_j$. Similarly, we assume that the second case has occurred if the edge $E_{V_iV_{i_0}}$ of $A(\sigma, t_{k+1})$ punctures a face $F_{\bar{j}_0}$, $\bar{j}_0\in\mathcal{F}_B^j$, of $B(\sigma, t_{k+1})$, and we predict the configuration $E_{V_iV_{i_0}}E_{F_jF_{\bar{j}_0}}$.

The prediction procedure is described as follows: Suppose that the conditions (8) hold, and suppose that *only* one of the inequalities of (9) is violated for $\bar{i}_0\in\mathcal{V}_A^i$, *i.e.*, $(-T_B^+\gamma_j)^TT_A^+(v_{\bar{i}_0}-v_i)>0$ under the assumption that C^+ is generic. Obviously, points along the edge $E_{V_iV_{\bar{i}_0}}$ of $A(\sigma, t_{k+1})$ are given by

$$\{y : y=\sigma T_A^+(v_i+\lambda(v_{\bar{i}_0}-v_i))+s_A^+,\ 0\leqslant\lambda\leqslant 1\}. \quad (26)$$

Thus, a point on the line segment is contained in the intersection of the closed half spaces bounded by the facial planes containing respectively the faces $F_{\bar{j}}$, $\bar{j}\in\mathcal{F}_B^j$, of $B(\sigma, t_{k+1})$ if and only if

$$(T_B^+\gamma_{\bar{j}})^T(\sigma T_A^+(v_i+\lambda(v_{\bar{i}_0}-v_i))+s_A^+-s_B^+)\leqslant\sigma,\ \bar{j}\in\mathcal{F}_B^j, \quad (27)$$

or, equivalently,

$$(T_B^+\gamma_{\bar{j}})^T(\sigma T_A^+(\lambda(v_{\bar{i}_0}-v_i))+x-s_B^+)\leqslant\sigma,\ \bar{j}\in\mathcal{F}_B^j \quad (28)$$

where $x=\sigma T_A^+v_i+s_A^+$; see (7). We need to determine the maximum value of λ, λ_{max}, such that all the inequalities (28) are satisfied. Note that: if $\lambda_{max}>1$, the edge does not puncture any one of the faces; if $\lambda_{max}<1$, the edge punctures the face (more precisely, the facial plane containing the face) which determines λ_{max}. Since the conditions (8) hold, *i.e.*, $(T_B^+\gamma_{\bar{j}})^T(x-s_B^+)<\sigma$, $\bar{j}\in\mathcal{F}_B^j$, it follows that: if $(T_B^+\gamma_{\bar{j}})^TT_A^+(v_{\bar{i}_0}-v_i)\leqslant 0$, the inequality in (28) is satisfied for all $\lambda\geqslant 0$. Thus, λ_{max} is given by

$$\lambda_{max}=\min_{\substack{\bar{j}\in\mathcal{F}_B^j\\(T_B^+\gamma_{\bar{j}})^T(T_A^+(v_{\bar{i}_0}-v_i))>0}}\frac{\sigma-(T_B^+\gamma_{\bar{j}})^T(x-s_B^+)}{(T_B^+\gamma_{\bar{j}})^T(\sigma T_A^+(v_{\bar{i}_0}-v_i))}. \quad (29)$$

Then: if $\lambda_{max}>1$, we determine the prediction $C=V_{\bar{i}_0}F_j$; if $\lambda_{max}<1$, we determine $C=E_{V_iV_{\bar{i}_o}}E_{F_{\bar{j}}F_{\bar{j}_0}}$ where $\bar{j}_0$ denotes the face index $\bar{j}$ which determines λ_{max} of (29); if $\lambda_{max}=1$, either of the predictions can be employed.

A similar discussion applies if the configuration at t_k is of an *EE* type. Suppose that the test procedures are entered at t_{k+1} with an *EE* configuration C^-. Using C^- with the object data at t_{k+1}, solve (14) and (15) for σ, λ_A, and λ_B and determine x. Suppose that (16)–(19), (22) and (25) are satisfied at t_{k+1}, and suppose that *only* (24) does not hold at t_{k+1}, *i.e.*, β_2, $\beta_1<0$ under the assumption that C^+ is generic. This is the case that the edge of $A(\sigma, t_{k+1})$ penetrates through x below one of the two faces of the edge of $B(\sigma, t_{k+1})$. In this case, the transition at $t=\bar{t}$ is generically of the *EF* type. Thus, the prediction idea for the case $C^-=V_iF_j$ can be applied similarly to this case. First we need to determine which one of the two faces of $B(\sigma, t_{k+1})$ is involved and which one of the two vertices of the edge of $A(\sigma, t_{k+1})$ has moved into the face. We can show that if β_2, $\beta_1<0$, either $(T_B^-\gamma_{B_1})^T(T_A^-e_A)\cdot(T_B^+\gamma_{B1})^T(T_A^+e_A)<0$ or $(T_B^-\gamma_{B2})^T(T_A^-e_A)\cdot(T_B^+\gamma_{B2})^T(T_A^+e_A)<0$ must hold. Furthermore, if $(T_B^-\gamma_{B_1})^T(T_A^-e_A)\cdot(T_B^+\gamma_{B1})^T(T_A^+e_A)<0$, then the face involved is of the face normal γ_{B1}; otherwise, the face is of the face of normal γ_{B2}. Let us denote the index of the face by j. Having determined the face, we can determine the vertex that has moved into the face by testing the sign of $(T_B^+\gamma_j)^T(T_A^+e_A)$: if the sign is positive, the vertex is of v_{A1}; if the sign is

https://doi.org/10.1017/S0263574799001939 Published online by Cambridge University Press

negative, it is of v_{A2}. Let us denote the index of the vertex by $\bar{i}_0$ and the other by i. Then, the procedure is the same as the preceeding *VF* case except that

$$\lambda_{max} = \min_{\substack{\bar{j}\in\mathcal{F}_B^j \\ (T_B^+\gamma_{\bar{j}})^T(\sigma T_A^+ \nu_{\bar{i}_0} + s_A^+ - x)>0}} \frac{\sigma - (T_B^+\gamma_{\bar{j}})^T(x - s_B^+)}{(T_B^+\gamma_{\bar{j}})^T(\sigma T_A^+ \nu_{\bar{i}_0} + s_A^+ - x)}. \quad (30)$$

If (22), instead of (24), does not hold at t_{k+1}, *i.e.*, $\alpha_2\alpha_1<0$, then the procedure is the same except for the interchange in the role of $A(\sigma, t_{k+1})$ and $B(\sigma, t_{k+1})$.

3.3. Prediction for infeasible configurations

In the preceding discussion, we have considered the prediction for the *EF*-type transition. Recall that we assume that the *EF* transition has occurred if a *VF* configuration is feasible but not regularly-separated. Now we will discuss the prediction procedures for the case that a *VF* configuration is not feasible. First, consider the geometric situation corresponding to infeasibility of a *VF* configuration. This is shown in Figure 4. The *VF* configuration C^- applied at t_{k+1} gives (σ, x) where V_i belongs to the facial plane containing F_j, but does not belong to $B(\sigma, t_{k+1})$. The transition configuration at $t=\bar{t}$ is generically of the *VE* type. For $A(\sigma, t_{k+1})$ and $B(\sigma, t_{k+1})$ to touch it is clear that σ must increase; when they do touch the likely generic configurations are $V_iF_{\bar{j}_o}$ or $E_{F_jF_{\bar{j}_0}}$ with one of the edges emanating from V_i. The configuration V_iF_j is impossible because the increase in σ means V_i is not contained in the facial plane of F_j. Note that the face $F_{\bar{j}_0}$ is predicted by one of the facial inequalities (8) which is violated by the loss of feasibility, *i.e.*, $F_{\bar{j}_0}$ is a face adjacent to F_j and $(T_B^+\gamma_{\bar{j}_0})^T(x - s_B^+) > \sigma$. We assume implicitly that *only* one facial inequality is violated, *i.e.*, $(T_B^+\gamma_{\bar{j}})^T(x - s_B^+) < \sigma$, $\bar{j}\in\mathcal{F}_B^j$, $\bar{j}\neq\bar{j}_0$. Generically, this is the situation if Δt is sufficiently small.

The prediction of the configuration at t_{k+1} is best understood in terms of the tangent cones of the objects defined by C^- and their corresponding normal cones. For example, let C^- be V_iF_j and assume that the vertex V_i has three adjacent vertices with indices $i_1, i_2, i_3 \in \mathcal{V}_A^i$, respectively. The normal cone geometry is displayed in Figure 5(a), looking "down" on $NC_A^-(V_i)$ "into" the vector $-T_B^-\gamma_j$ emanating upwards from the origin. The figure indicates the vectors $T_A^-(v_{i1} - v_i)$, $T_A^-(v_{i2} - v_i)$, and $T_A^-(v_{i3} - v_i)$, which are outward normal to each corresponding face of $NC_A^-(V_i)$. The shaded triangle represents the intersection of $NC_A^-(V_i)$ with a plane lying "above" the origin. The dots show where the plane intersects the ray emnating from the origin in the directions $-T_B^-\gamma_j$. From Figure 5(a), $-T_B^-\gamma_j \in riNC_A^-(V_i)$, so that indeed there is V_iF_j configuration at t_k. As the objects move to their positions at t_{k+1}, the normal cone picture changes slightly because $T_A^- \to T_A^+$ and $T_B^- \to T_B^+$. The resulting new picture is the basis for predicting C^+. The two possible transitions that can occur from the loss of feasibility of (σ, x) at t_{k+1} are illustrated in Figure 5(b) and (c). The transition to a new *VF* configuration is characterized by $-T_B^+\gamma_{\bar{j}_0} \in riNC_A^-(V_i)$ (Figure 5(b)). Note that $-T_B^+\gamma_j$ is *not* involved in the determination of C^+ since it corresponds to the facial constraint by which feasibility was lost. The transition to an *EE* configuration is characterized by $-T_B^+\gamma_j \in riNC_A^+(V_i)$ and $-T_B^+\gamma_{\bar{j}_0} \notin NC_A^+(V_i)$ (Figure 5(c)). The resulting *EE* configuration is determined by $riNC_A^+(E_{V_iV_{i1}}) \cap -riNC_B^+(E_{F_jF_{\bar{j}_0}}) \neq \phi$. The intersection of *only two* fan-like cones, *i.e.*, a unique prediction of contact configuration, is assured by $-T_B^+\gamma_j \in riNC_A^+(V_i)$ and $-T_B^+\gamma_{\bar{j}_0} \notin NC_A^+(V_i)$. Since $-T_B^-\gamma_j$ is contained in $riNC_A^-(V_i)$, $-T_B^+\gamma_j$ is contained in $riNC_A^+(V_i)$ under the assumption that the regular separation conditions (9) are

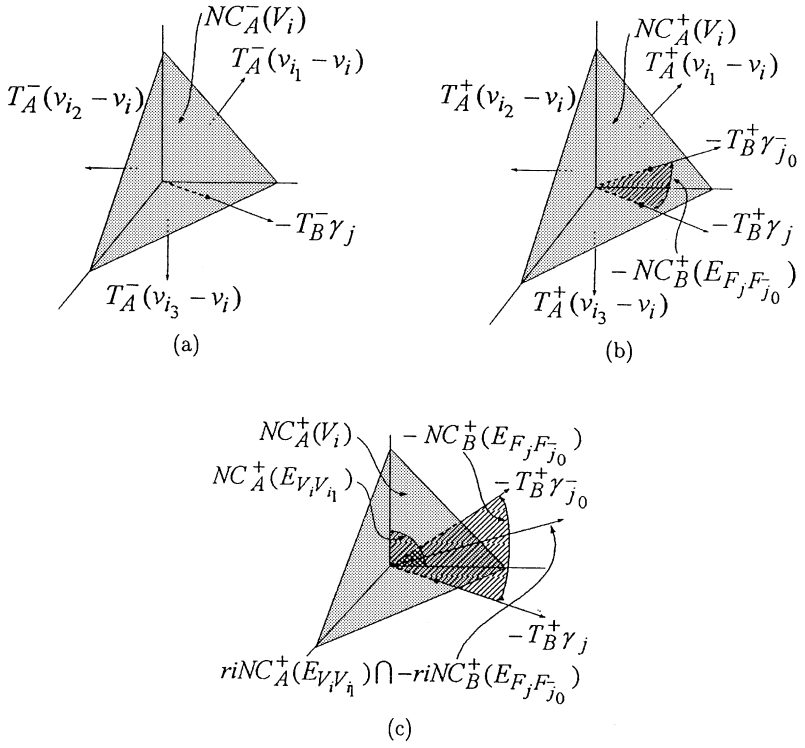

Fig. 5. Normal cone transitions for an infeasible *VF* configuration. (a) $C^- = V_iF_j$. (b) $C^+ = V_iF_{\bar{j}_0}$. (c) $C^+ = E_{V_iV_{i_1}}E_{F_jF_{\bar{j}_0}}$.

https://doi.org/10.1017/S0263574799001939 Published online by Cambridge University Press

satisfied for sufficiently small Δt. Thus, the transition determination implicit in the preceding dicussion is valid if Δt is sufficiently small.

The transition determination is described as follows: Suppose that the regular separation conditions (9) are satisfied, *i.e.*, $-T_B^+\gamma_j \in riNC_A^+(V_i)$, and suppose that *only* one inequality of the feasibility conditions (8) is violated for $\bar{j}_0 \in \mathcal{F}_B^j$, *i.e.*, $(T_B^+\gamma_{j_0})^T(x-s_B^+) > \sigma$ under the assumption that C^+ is generic. We need to determine whether or not the fan-like cone $-NC_B^+(E_{F_jF_{j_0}})$ intersects any face of the normal cone $NC_A^+(V_i)$, and, if it does, what face of $NC_A^+(V_i)$ the fan-like cone intersects. Note that $-NC_B^+(E_{F_jF_{j_0}}) = \{y : y = \alpha(-T_B^+\gamma_j + \lambda(-T_B^+(\gamma_{\bar{j}} - \gamma_j))),$ $\alpha > 0,\ 0 \le \lambda \le 1\}$. A half-line in $-NC_B^+(E_{F_jF_{j_0}})$ is contained in $NC_A^+(V_i)$ if and only if

$$(T_A^+(v_{\bar{i}} - v_i))^T(-T_B^+\gamma_j + \lambda(T_B^+(\gamma_{\bar{j}_0} - \gamma_j))) \le 0,\ \bar{i} \in \mathcal{V}_A^i. \quad (31)$$

Let λ_{max} denote the maximum value of λ such that all the inequalities (31) are satisfied. Note that: if $\lambda_{max} > 1$, $-T_B^+\gamma_{\bar{j}_0} \in riNC_A^+(V_i)$; if $\lambda_{max} < 1$, $-T_B^+\gamma_{\bar{j}_0} \notin NC_A^+(V_i)$ and $-NC_B^+(E_{F_jF_{\bar{j}_0}})$ intersects a face of $NC_A^+(V_i)$ which determines λ_{max}. Since the conditions (9) hold, *i.e.*, $(-T_B^+\gamma_j)^T T_A^+(v_{\bar{i}} - v_i) < 0$, $\bar{i} \in \mathcal{V}_A^i$, it follows that: if $(T_A^+(v_{\bar{i}} - v_i))^T(-T_B^+(\gamma_{\bar{j}_0} - \gamma_j)) \le 0$, the inequality in (31) is satisfied for all $\lambda \ge 0$. Thus, γ_{max} is given by

$$\lambda_{max} = \min_{\substack{\bar{i} \in \mathcal{V}_A^i \\ (T_A^+(v_{\bar{i}} - v_i))^T(-T_B^+(\gamma_{\bar{j}_0} - \gamma_j)) > 0}} \frac{(T_A^+(v_{\bar{i}} - v_i))^T(T_B^+\gamma_j)}{(T_A^+(v_{\bar{i}} - v_i))^T(-T_B^+(\gamma_{\bar{j}_0} - \gamma_j))}. \quad (32)$$

Then: if $\lambda_{max} > 1$, we determine the prediction $C = V_i F_{\bar{j}_0}$; if $\lambda_{max} < 1$, we determine $C = E_{V_iV_{\bar{i}_0}}E_{F_jF_{\bar{j}_0}}$ where $\bar{i}_0$ denotes the vertex index $\bar{i}$ which determines λ_{max} of (32). If $\lambda_{max} = 1$, there is a possibility that C^+ is nongeneric and the prediction is indeterminate.

A similar discussion applies if the configuration at t_k is of an *EE* type. Feasibility is lost at t_{k+1} if the two infinite lines extending along the two edges intersect at (σ, x) and x does not belong to one of the edges. The transition configuration is then of type *VE* where the edge is one of the original edges (the one which x belongs) and V is a vertex at the end of the other edge (the vertex corresponding to the end of the edge which is closest to x). Again, generically for small Δt, contact of $A(\sigma, t_{k+1})$ and $B(\sigma, t_{k+1})$ requires an increase in σ and two types of contact can occur: E with one of the other edges of V and V with one of the faces adjoining E.

More specifically, let C^- be $E_{V_jV_{i_1}}E_{F_{j_1}F_{j_2}}$ configuration. Of course, the vertex pair V_i, V_{i_1} and the face pair F_{j_1}, F_{j_2} define the edges of $A(\sigma_k^*, t_k)$ and $B(\sigma_k^*, t_k)$ in contact, respectvely. Suppose that the test procedures are entered at t_{k+1} with the *EE* configuration C^-. Using C^- with the object data at t_{k+1}, we obtain (σ, x) as the intersection of σ-dependant lines extending from the edge $E_{V_iV_{i_1}}$ of $A(t_{k+1})$ and the edge $E_{F_{j_1}F_{j_2}}$ of $B(\sigma, t_{k+1})$. Suppose that feasibility is lost at t_{k+1} because x lies beyond a vertex of the edge of $A(\sigma, t_{k+1})$, and suppose, for example, that the vertex of $A(\sigma, t_{k+1})$ is V_i and it is adjacent to three vertices. Clearly, one of them is V_{i1}; let V_{i_2}, V_{i_3} denote the other two vertices. Then arrangement of the normal cones is shown in Figure 6. The picture of the normal cones are depicted in same manner as in Figure 5; however, for simplicity the vectors $T_A^+(v_{\bar{i}} - v_i)$, $\bar{i} = i_1, i_2, i_3$, which are outward normal to a corresponding face of $NC_A^+(V_i)$, are not shown. The resulting *VF* and *EE* configurations at t_{k+1} do not involve the edge $E_{V_iV_{i_1}}$ because it is the edge on which feasibility is lost. Note that $-T_B^+\gamma_{j_1}$ and $-T_B^+\gamma_{j_2}$ can't both be in $NC_A^+(V_i)$ if Δt is sufficiently small; the cones $NC_A^-(E_{V_iV_{i_1}})$ and $-NC_B^-(E_{F_{j_1}F_{j_2}})$ intersect in their relative interiors and the same must be said for $NC_A^+(E_{V_iV_{i_1}})$ and $-NC_B^+(E_{F_{j_1}F_{j_2}})$. Suppose as in Figure 6(b), $-T_B^+\gamma_{j_2} \notin NC_A^+(V_i)$. Then, there are two possibilities: $-T_B^+\gamma_{j_1} \in NC_A^+(V_i)$ and $-T_B^+\gamma_{j_1} \notin NC_A^+(V_i)$. The arguments are not changed in substance if $-T_B^+\gamma_{j_1} \notin NC_A^+(V_i)$ and

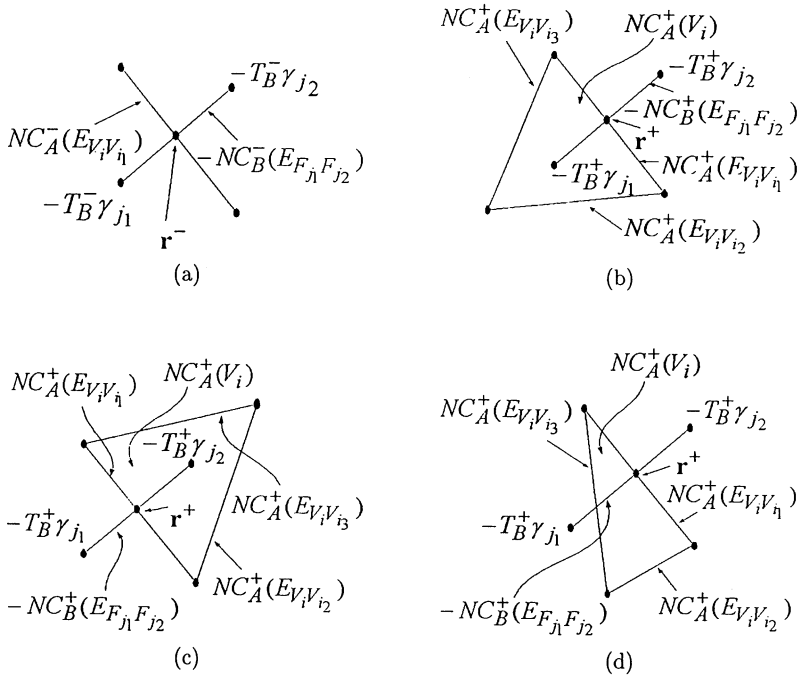

Fig. 6. Normal cone transitions for an infeasible *EE* configuration. $\mathbf{r}^- = riNC_A^-(E_{V_jV_{i_1}}) \cap -riNC_B^-(E_{F_{j_1}F_{j_2}})$ and $\mathbf{r}^+ = riNC_A^+(E_{V_iV_{i_1}}) \cap -riNC_B^+(E_{F_{j_1}F_{j_2}})$. (*a*) $C^- = E_{V_jV_{i_1}}E_{F_{j_1}F_{j_2}}$. (b) $C^+ = V_iF_{j_1}$. (c) $C^+ = V_iF_{j_2}$. (d) $C^+ = E_{v_iv_{i_3}}E_{F_{j_1}F_{j_2}}$.

https://doi.org/10.1017/S0263574799001939 Published online by Cambridge University Press

$-T_B^+\gamma_{j_2} \in NC_A^+(V_i)$; see Figure 6(c). The first possibility implies the $V_iF_{j_1}$ configuration (Figure 6(b)); the second implies an EE configuration where the new edge is determined by where $-NC_B^+(E_{F_{j_1}F_{j_2}})$ intersects the normal cone $NC_A^+(E_{V_iV_{i_3}})$ that is a face of $NC_A^+(V_i)$ (Figure 6(d)). In fact, the face of $NC_A^+(V_i)$ has the outward normal vector $T_A^+(v_{i_3} - v_i)$. Because of the convexity of the normal cones, generically there can only be one such face of $NC_A^+(V_i)$. Thus, in both *VF* and *EE* cases the prediction is uniquely determined.

The transition determination is stated as follows: Suppose that the test procedures are entered at t_{k+1} with $C^- = E_{V_iV_{i_1}}E_{F_{j_1}F_{j_2}}$. Suppose that *only* one of either (16) or (17) is violated among the feasibility conditions (16)–(19), and suppose that all the regular separation conditions (22), (24) and (25) are satisfied. If (16) is violated, *i.e.*, $\lambda_A < 0$ under the assumption that C^+ is generic, the transition configuration is generically of type *VE* and the vertex involved is of v_{A_1}. If, (17), instead of (16), is violated, *i.e.*, $\lambda_A > 1$, the vertex involved is of v_{A_2}. Without, loss of generality, let us denote the vertex by V_i. First, we need to determine which movement from $\mathbf{r}^+ = riNC_A^+(E_{V_iV_{i_1}}) \cap -riNC_B^+(E_{F_{j_1}F_{j_2}})$ toward $-T_B^+\gamma_{j_1}$ or $-T_B^+\gamma_{j_2}$ directs toward inside of $NC_A^+(V_i)$. This question is answered easily. Since $T_A^+(v_{i_1} - v_i)$ is the outward normal to the face $NC_A^+(E_{V_iV_{i_1}})$ of $NC_A^+(V_i)$, it follows that: if $(T_A^+(v_{i_1} - v_i))^T(-T_B^+\gamma_{j_1}) < 0$, then the direction is toward $-T_B^+\gamma_{j_1}$; if $(T_A^+(v_{i_1} - v_i))^T(-T_B^+\gamma_{j_2}) < 0$, then it is toward $-T_B^+\gamma_{j_2}$. Having decided the direction, the transition determination is similar to the infeasible *VF* case. If the direction is toward $-T_B^+\gamma_{j_1}$, we need to determine if $-T_B^+\gamma_{j_1} \in riNC_A^+(V_i)$, and, if not, what face of $NC_A^+(V_i)$, except the face $NC_A^+(E_{V_iV_{i_1}})$, is intersected by the fan-like cone $-NC_B^+(E_{F_{j_1}F_{j_2}})$. Since $-NC_B^+(E_{F_{j_1}F_{j_2}}) = \{y : y = \alpha(-T_B^+\gamma_{j_2} + \lambda(-T_B^+(\gamma_{j_1} - \gamma_{j_2}))),\ \alpha > 0,\ 0 \le \lambda \le 1\}$, a half-line in $-NC_B^+(E_{F_{j_1}F_{j_2}})$ is contained in $NC_A^+(V_i)$ if and only if

$$(T_A^+(v_{\bar{i}} - v_i))^T(-T_B^+\gamma_{j_2} + \lambda(-T_B^+(\gamma_{j_1} - \gamma_{j_2}))) \le 0,\ \bar{i} \in \mathcal{V}_A^i. \quad (33)$$

Let λ_{max} denote the maximum value of λ such that all the inequalities (33) are satisfied. Note that λ_{max} is determined by a face of $NC_A^+(V_i)$ where the half-line is leaving behind $NC_A^+(V_i)$ as λ increases. That is, λ_{max} is determined for $\bar{i} \in \mathcal{V}_A^i$ such that $(T_A^+(v_{\bar{i}} - v_i))^T(-T_B^+(\gamma_{j_1} - \gamma_{j_2})) > 0$. Since there exists a $\lambda > 0$ such that (33) holds for all $\bar{i} \in \mathcal{V}_A^i$, $(T_A^+(v_{\bar{i}} - v_i))^T(-T_B^+(\gamma_{j_1} - \gamma_{j_2})) > 0$ implies $(T_A^+(v_{\bar{i}} - v_i))^T(-T_B^+\gamma_{j2}) < 0$. Accordingly, λ_{max} is given by

$$\lambda_{max} = \min_{\substack{\bar{i} \in \mathcal{V}_A^i \\ (T_A^+(v_{\bar{i}} - v_i))^T(-T_B^+(\gamma_{j_1} - \gamma_{j_2})) > 0}} \frac{(T_A^+(v_{\bar{i}} - v_i))^T(T_B^+\ \gamma_{j_2})}{(T_A^+(v_{\bar{i}} - v_i))^T(-T_B^+(\gamma_{j_1} - \gamma_{j_2}))} \quad (34)$$

If $\lambda_{max} > 1$, we determine the prediction $C = V_iF_{j_1}$; if $\lambda_{max} < 1$, then we determine $C = E_{V_iV_{\bar{i}_0}}\ E_{F_{j_1}F_{j_2}}$ where $\bar{i}_0$ denotes the vertex index $\bar{i}$ which determines λ_{max} of (34); if $\lambda_{max} = 1$, there is a possibility that C^+ is nongeneric and the prediction is indeterminate. If the direction is toward $-T_B^+\gamma_{j_2}$, then the preceding arguments apply with γ_{j_1} and γ_{j_2} being interchanged. If either (18) or (19) is violated, the arguments are not changed in substance except for the interchange in the role of $A(\sigma, t_{k+1})$ and $B(\sigma, t_{k+1})$.

3.4. The incremental growth distance algorithm (IGDA)

One iteration of our IGDA algorithm is described as follows: (1) Given C^-, set C to C^- and enter the test procedures; (2) If $C = C^+$, then return C^+ and $(\sigma^*_{k+1}, x^*_{k+1})$; otherwise, enter the prediction procedures to determine C; (3) If C is determinate, enter restart steps to return C^+ and $(\sigma^*_{k+1}, x^*_{k+1})$. (4) Given C, enter the test procedures; (5) If $C = C^+$, then return C^+ and $(\sigma^*_{k+1}, x^*_{k+1})$; otherwise, enter restart steps to return C^+ and $(\sigma^*_{k+1}, x^*_{k+1})$.

The input arguments of IGDA at each iteration are the quadruple $(T_A^+, s_A^+, T_B^+, s_B^+)$ and C^-. IGDA returns C^+ and $(\sigma^*_{k+1}, x,^*_{k+1})$. For the initial point of a given path, C^- is not available and we must use restart steps to determine C^- and (σ^*_0, x^*_0). For simplicity, we did not include the step to scale σ^* appropriately to generate the separation and penetration growth distances. Recall that, for example, the penetration growth distance is simply obtained by scaling $1 - \sigma^*$ according to the size of $\bar{A}$ and $\bar{B}$.

Note that the prediction procedures of IGDA can determine a "likely" C^+ when either *only* one inequality of (8), (9) or *only* one of (16)–(19), (22), (24) is violated. That can occur where there is only one transition time between t_k and t_{k+1}. We can circumvent this requirement by assigning some points between t_k and t_{k+1} so that the requirement can be satisfied and, thus, the prediction is possible for each pair of adjacent (assigned) points and so the prediction of C^+ is eventually possible. Each point is assigned sequentially and its location can be selected adaptively based on results of prediction and verification at previously assigned points. However, such a scheme seems not required for incremental motions of our interest where the prediction of IGDA is almost always possible and correct.

The computational complexity of the test procedures is $O(|\mathcal{V}_A^i| + |\mathcal{F}_B|)$ for the *VF* configuration, and it is a constant for *EE* configurations. The complexity of the prediction procedures is $O(|\mathcal{F}_B|)$ for the non-optimal configuration and $O(|\mathcal{V}_A^i|)$ for the infeasible configuration. That is, the computational complexity of the test and prediction procedures depends on the local geometric complexity of two polytopes. It is very difficult to predict a precise computation time for IGDA, because the time depends on the geometric complexity of polytopes, the complexity of motion, and the number of grid points along the path which specifies the motion. The number of contact transitions increases as the complexities of polytopes and their motion increase. Consider the situation that grid points are closely-spaced so that there is at most one transition between each pair of adjacent grid points. In this situation, the prediction rarely fails and as rarely restart steps are brought into play. Furthermore, if the number of contact transitions is a small fraction of the number of grid points, only a test procedure is executed at most of the grid points to confirm that $C^- = C^+$. In this case the computation time of IGDA, in average, is determined by the execution time of the test procedures which depends on the local geometric complexity.

We can reduce further the computation time required for the test procedures. Consider that the conditons (8) are tested for the *VF* configuration. The computation time for this testing is $O(|\mathcal{F}_B|)$. If the face F_j of $\bar{B}$ is complex, *i.e.*,

https://doi.org/10.1017/S0263574799001939 Published online by Cambridge University Press

$|\mathcal{F}_B|$ is large, it causes difficulties in fast implementation of IGDA. Alternatively, we can divide the complex face into a set of subfaces. Using the facial subdivision, the computation time required for the feasibility test can be reduced substantially for complex faces. We implemented in IGDA the feasibility test procedure which takes advantage of facial subdivision data. The idea of the facial subdivision can be applied in testing the separation conditions (9): the normal cone of a complex vertex can be decomposed into a set of simple cones. As a result, the total computational time of IGDA for a closely-spaced grid does not depend significantly on object complexity. Numerical experiments confirm this. Similar subdivision structures have been used in reference 7.

4. NUMERICAL EXPERIMENTS

We implemented IGDA in *C*-language. Many numerical computations have been performed. They involved a variety of different objects in R^3 with $(|\mathcal{F}_A| + |\mathcal{F}_B|)$ ranging between 8 and 200. The objects include various simple polytopes, an isocosahedron, a Bucky ball with 12 pentagons and 20 hexagons as its faces, and circular right cylinders approximated by polytopes with 40 and 100 faces. All objects were contained within outer sphere of radius 5. A facial subdivision was employed for a complex faces of the right cylinders with 40 and 100 faces.

Object A moves along a straight line path from $(-10, 0.5, 10)$ to $(10, 0.5, 10)$ and rotating at a constant rate. The rotation was generated by using an Euler angle parametrization of $SO(3)$ and increasing linearly the angles from 0 to π. Object B is fixed at the origin with the angles from a uniform distribution on $[-\pi, \pi]$. For each object pair 100 paths were generated each with the random orientation of the object B. For each of nearly 150 object pairs, the numbers of contact transitions were obtained and averaged over the 100 paths. The average number is nearly linear with respect to the total number of faces, and is given approximately by $0.75(|\mathcal{F}_A| + |\mathcal{F}_B|)$.

The C-language code, with an optimal run-time compilation, was run on an HP 9000/710 (50 MHz) to evaluate the growth distances on an equally-spaced grid of 1000 points along each path. The test and prediction procedures succeeded for most of the 1000 grid points: they failed, in average over the 100 paths, at less than one point for 1000 grid–points. Except at such points, the average computation times at each grid point were between 100 microseconds and 160 microseconds; see Figure 7. For finer grids, the computation time increased slightly from 100 microseconds to 120 microseconds as the number of faces of two objects increases. The results confirm that the average computation times depend little on the geometric complexity of two polytopes. When the grids are coarser, the computation time can increase more noticeably as the object complexity increases. Not surprisingly, this is due to the fact that our test and prediction procedures can have more chances to fail as the grids become coarser and as the object complexity increases. The coarser grids, however, are not the case that IGDA is intended to apply to.

Using an active set method (LP)[13] with a special initialization[1,2], we solved the full linear programming problem (3) to obtain the total computational times for the 1000 grid-point paths. We compared the total computation times to the IGDA's. The comparison shows that IGDA is faster by ratios that are approximated by $0.25(|\mathcal{F}_A| + |\mathcal{F}_B|)$ (Figure 8): the speed advantage is more significant as object complexity increases. A simple scheme, which exploits the coherence of contact configurations in incremental motions, has been discussed in references 1 and 2. However, the scheme, called maintaining active constraints (MAC), takes $O(|\mathcal{F}_A| + |\mathcal{F}_B|)$ time because it does not take advantage of geometric adjancency structures. We also obtained the total

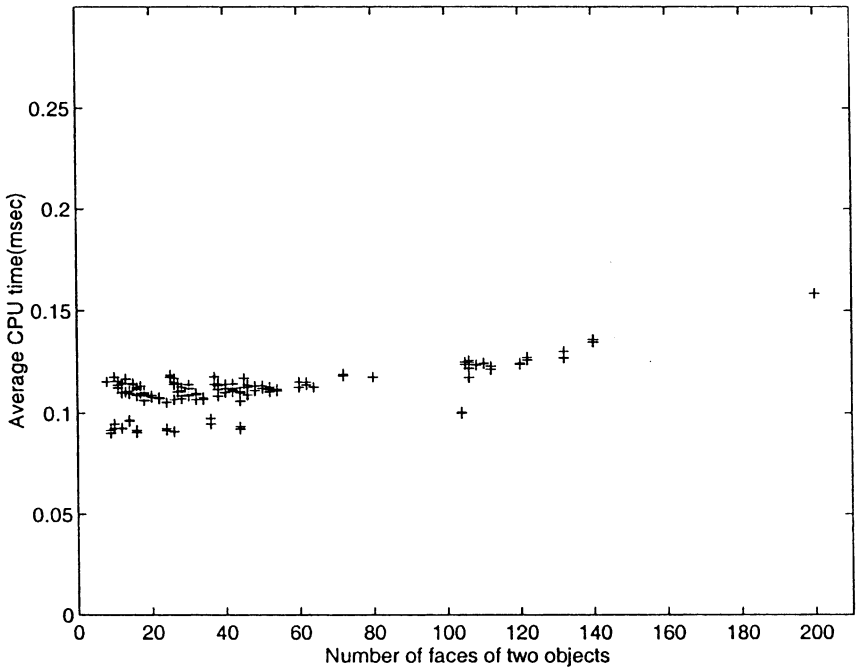

Fig. 7. Average computational time at each grid point (for 1000 grid-point paths).

https://doi.org/10.1017/S0263574799001939 Published online by Cambridge University Press

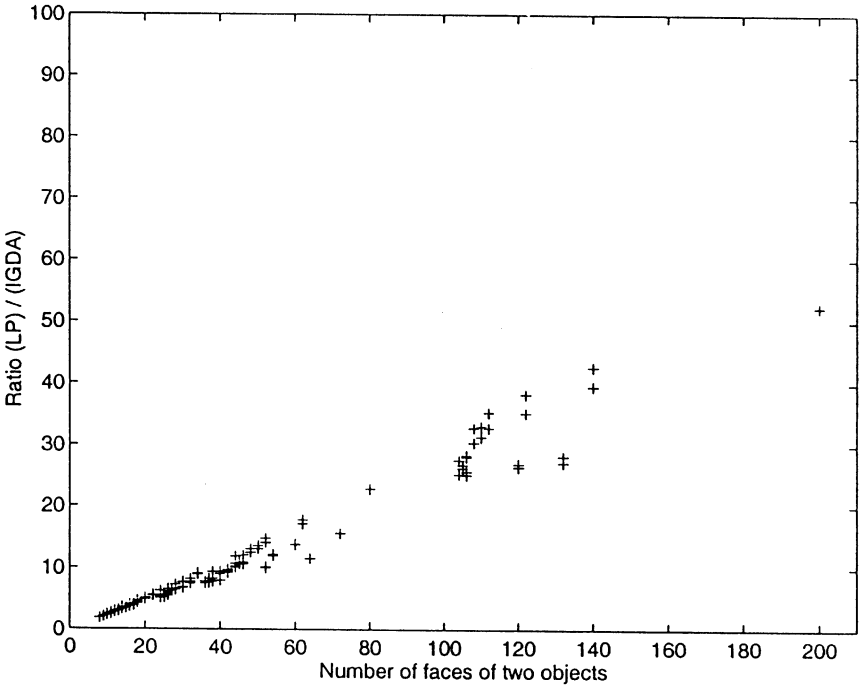

Fig. 8. Ratio of average computational times (LP)/(IGDA).

computational times of MAC for the 1000 grid-point paths. As expected, IGDA is faster approximately by the ratios of $0.05(|\mathcal{F}_A|+|\mathcal{F}_B|)$, but not less than one, than MAC; see Figure 9. Note that IGDA is approximately 10 times faster than MAC when the total number of faces is 200. We compared IGDA with Ong and Huang's incremental version[6] with respect to the number of arithematic operations required for an asymptotic case where motion increments are sufficiently small. The result indicates that IGDA requires approximately 20% less operations than Ong and Huang's version.

We applied IGDA to solve an interference detection problem which is a typical problem in robotic and graphic simulations. Consider a situation that a six-axis PUMA robot (reference 13, p.37) is moving a payload along a path between two obstacles. The payload is a dumbbell with Bucky balls on either side, and the obstacles are a pair of 100-face rectangular cyclinders. Figure 10 shows the trajectory of the payload that moves from the left to the right position along a path between the rectangular cylinder pair. The path is specified by a straight line connecting the starting point (1.904, −0.393, 2.444, −3.142, 2.051, 1.238) [rad] and the destination point (0.866, −0.518, −2.411, 0.000, 1.248, 0.866) [rad] in the joint space of the

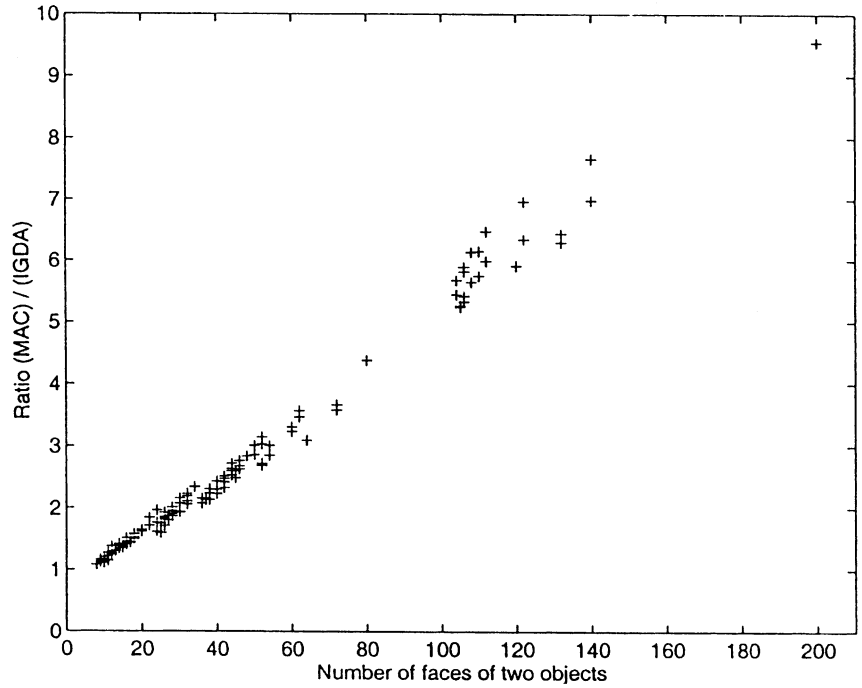

Fig. 9. Ratio of average computational times (MAC)/(IGDA).

https://doi.org/10.1017/S0263574799001939 Published online by Cambridge University Press

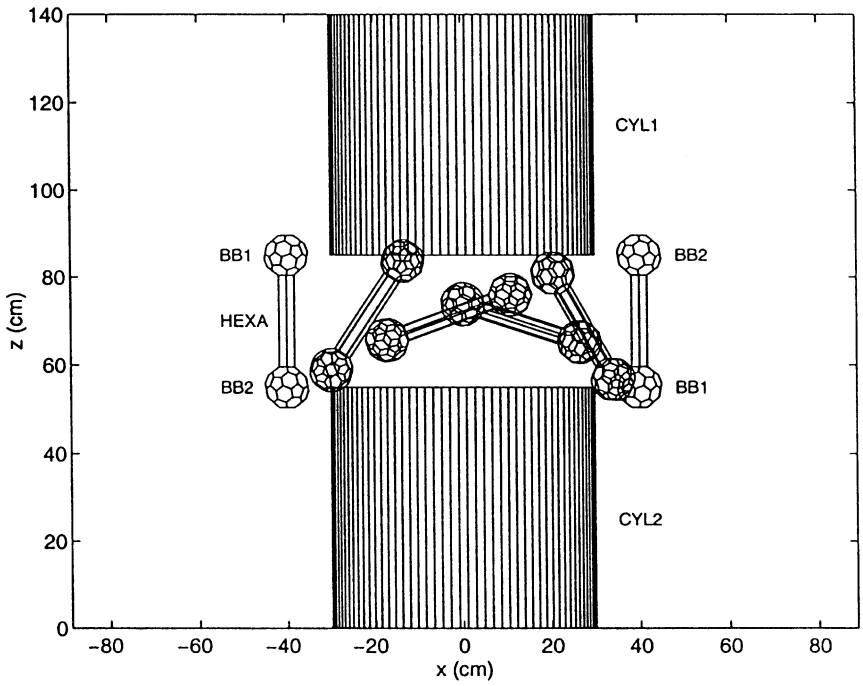

Fig. 10. Trajectory of the payload.

PUMA robot. We obtained the interfering intervals along the path by computing the growth distance between each element pair of the payload and the obstacles at 1000 equally-spaced grid points along the path. The growth distance is presented in Figure 11 for each object pair. The positive value of the growth distance implies no interference between the corresponding object pair at the grid point. The figure shows that, for example, a Bucky ball (BB1) and the upper cylinder (CYL1) intersect each other at the grid points between [45, 298], but the Bucky ball (BB1) and the lower cylinder (CYL2) does not intersect each other at all. On HP 9000/710, the computation time of IGDA was 1.23 sec that was required to solve this inteference detection problem. For LP and MAC, the computation times were 49.8 sec and 7.62 sec, respectively. It implies that IGDA is faster than LP and MAC, respectively, by aproximately 40 and 6 times in solving this problem. This result is consistant with our experimental results above.

5. CONCLUSION

A numerical procedure has been presented for computing incremental growth distances between a pair of polytopes.

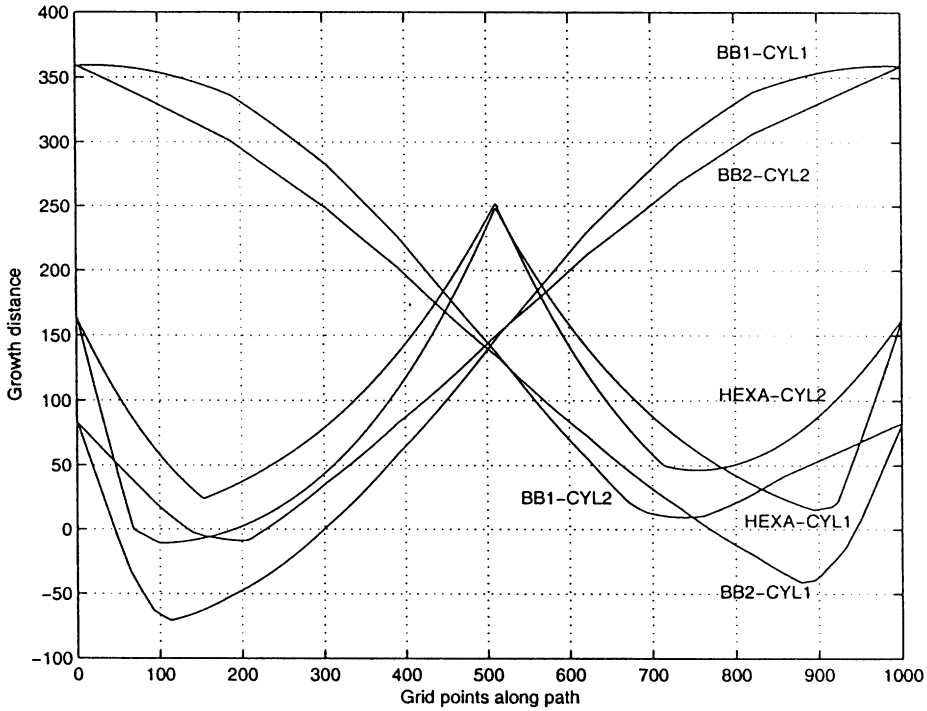

Fig. 11. Growth distance between each pair of payload and obstacle elements.

https://doi.org/10.1017/S0263574799001939 Published online by Cambridge University Press

The procedure uses vertex and facial characterizations of polytopes and exploits their geometric adjacency information. Preprocessing of the data structure is required.The average time of computation for incremental motions is very small and does not depend significantly on object complexity. An interference detection problem was solved using our procedure to demonstrate its applicability to robotic simulations.

References

1. E.G. Gilbert and C.J. Ong, "New distances for the separation and penetration of objects" *Proc. IEEE Int. Conf. on Robotics and Automation*, San Diego, CA (May, 1994) pp. 579–586.
2. C.J. Ong and E.G. Gilbert, "Growth distances: new measures for object separation and penetration" *IEEE Trans. on Robotics and Automation* **RA–12,** No. 6, 888–903 (1996).
3. C.E. Buckley, "A proximity metric for continuum path planning" *Proc. 9th Int. Conf. on Artificial Intelligence* (1985) pp. 1096–1102.
4. C.E. Buckley, "A foundation for the 'flexible–trajectory' approach to numeric path planning" *Int. J. Robotics Res.* **8**, No. 3, 44–64 (1989).
5. C.J. Ong and E.G. Gilbert, "Robot path planning with penetration growth distance" *IEEE Int. Conf. on Robotics and Automation*, San Diego, CA (May, 1994) pp. 2146–2152.
6. C.J. Ong and E. Huang, "An incremental version of growth distance" *Proc. IEEE Int. Conf. on Robotics and Automation*, Leuven, Belgium (May, 1998) pp. 3671–3677.
7. M.C. Lin and J.F. Canny, "A fast algorithm for incremental distance calculation" *Proc. IEEE Int. Conf. on Robotics and Automation*, Sacramento, CA (May, 1991) pp. 1008–1014.
8. S. Cameron, "Enhancing GJK: computing minimum and penetration distances between convex polyhedra" *Proc. IEEE Int. Conf. on Robotics and Automation*, Albuquerque, NM (May, 1997) pp.3112–3117.
9. S. Cameron, "A comparison of two fast algorithms for computing the distances between convex polyhedra" *IEEE Trans. on Robotics and Automation* **RA–13**, No 6, 915–920 (1997).
10. C.J. Ong and E.G. Gilbert, "The Gilbert-Johnson-Keerthi distance algorithm: a fast version for incremental motions" *Proc. IEEE Int. Conf. on Robotics and Automation*, Albuquerque, NM (May, 1997) pp.1183–1189.
11. R.T. Rockafellar, *Convex Analysis* (Princeton Univ. Press, Princeton, NJ, 1970).
12. M.J. Best and K. Ritter, *Linear Programming: Active set Analysis and Computer Programs* (Pretence-Hall, Englewood Cliffs, NJ, 1985).
13. K.S. Fu, R.C. Gonzalez and C.S.G. Lee, *Robotics: Control, Sensing, Vision and Intelligence* (McGraw-Hill, New York, 1987).

https://doi.org/10.1017/S0263574799001939 Published online by Cambridge University Press